RSC Advances

PAPER

View Article Online
View Journal | View Issue

Cite this: *RSC Adv.*, 2025, **15**, 24142

Engineering solvent resistance in semiconducting polymer films through UV-induced polydiacetylene crosslinking†

Amit K. Sur, [a] Audithya Nyayachavadi,[a] Piumi Kulatunga,[a] Nien-Jung Li,[b] Yu-Cheng Chiu [b] and Simon Rondeau-Gagné *[a]

Semiconducting polymers have emerged as versatile, tunable materials for next-generation optoelectronic devices, offering advantages over traditional inorganic semiconductors in applications from energy harvesting to bioelectronics. Particularly, their compatibility with scalable manufacturing techniques, including solution-based deposition and printing methods, positions them favorably for commercial adoption. Among the recent strategies used to enhance the mechanical, thermal, and electronic properties of these polymers, crosslinking—through covalent or non-covalent interactions—has been shown to be especially efficient for improving their stability, robustness, and functionality. Notably, crosslinking can also confer solvent resistance to these materials, a crucial feature for multilayer device fabrication that can help to maintain layer integrity during sequential printing processes. In this work, we synthesized a diketopyrrolopyrrole–carbazole conjugated copolymer functionalized with 1,3-butadiyne groups on the carbazole side chains, enabling covalent crosslinking *via* UV-induced topochemical polymerization into polydiacetylene (PDA) networks. Raman spectroscopy confirmed PDA crosslink formation, while atomic force microscopy and grazing incidence wide-angle X-ray scattering were used to demonstrate the preservation of polymer film morphology post-crosslinking. Quantitative nanomechanical mapping revealed significant enhancements in mechanical properties upon PDA formation. Additionally, sequential deposition and crosslinking cycles demonstrated the robust solvent resistance of crosslinked films, confirmed by UV-vis spectroscopy. These results highlight topochemical polymerization of diacetylenes as an effective strategy for engineering mechanically robust, solvent-resistant conjugated polymer films suitable for advanced multilayer organic electronics.

Received 5th April 2025
Accepted 28th June 2025

DOI: 10.1039/d5ra02367j

rsc.li/rsc-advances

Introduction

In recent years, conjugated semiconducting polymers have emerged as promising materials for a wide array of optoelectronic devices, offering a compelling alternative to traditional inorganic semiconductors. Extensive research and development in organic electronics has showcased these polymers' remarkable versatility and synthetic tunability, paving the way for a novel toolkit of soft, deformable technologies with applications ranging from energy harvesting to bioelectronics. Moreover, their compatibility with large-scale manufacturing – through methods such as continuous-flow synthesis, high-throughput characterization, and solution deposition techniques like printing – provides a cost-effective and efficient route to next-generation device fabrication.[1–3]

In many emerging applications, device performance and market adoption are closely tied to the stability and compatibility of the materials used. Among other strategies, enhancing the thermal, mechanical, and electronic properties of semiconducting materials through polymer crosslinking has emerged as an effective approach.[4] Realized through the formation of new covalent and non-covalent bonds between individual polymer chains, crosslinking can improve material robustness and enable precise tuning of key physical properties of the materials by either modifying the degree of crosslinking or the nature of the crosslinks.[5,6] Covalent crosslinking techniques, including photochemical and thermal crosslinking with azide-containing crosslinkers, were shown to provide semiconducting materials with improved mechanical properties while preserving their favourable electronic properties.[7–9] Non-covalent crosslinking methods, which often rely on hydrogen bonding or ionic interactions, were also shown to facilitate

[a]*Department of Chemistry and Biochemistry, University of Windsor, 401 Sunset Avenue, Windsor, Ontario N9B 3P4, Canada. E-mail: srondeau@uwindsor.ca*

[b]*Department of Chemical Engineering, National Taiwan University of Science and Technology, Taipei 106, Taiwan*

† Electronic supplementary information (ESI) available: Experimental procedures; nuclear magnetic resonance spectra; Fourier-transform infrared spectra; Raman spectra; UV-vis spectra; GIWAXS spectra; AFM images; cyclic voltammograms; TGA spectra; quantitative nanomechanical mapping spectra. See DOI: https://doi.org/10.1039/d5ra02367j

reversible bond formation and to offer dynamic, stimuli-responsive behaviour to semiconducting polymers.[10]

Another key advantage of polymer crosslinking in semiconducting polymers is the development of solvent-resistant polymer films, which is often crucial for solution-based printing processes like inkjet, roll-to-roll, or screen printing. This engineered solvent resistance is particularly important in multilayer device fabrication to ensure that each printed layer remains chemically intact during the deposition of subsequent layers, thereby preserving overall device performance and enabling the fabrication of complex multi-layer architectures.[11] One common approach to impart solvent resistance for orthogonal semiconducting polymer processing involves modifying the polymer with an ester or carboxylic acid-containing alkyl chain that can subsequently be hydrolyzed to convert the film into one that is resistant to various organic solvents.[12,13] An alternative strategy involves incorporating a cleavable or crosslinkable side chain that, upon post-deposition treatments such as heating or UV exposure, either cleaves or crosslinks across adjacent polymer chains.[14]

To develop novel crosslinked semiconducting polymer systems, our group and others have introduced a new method to covalently crosslink high-performance semiconducting π-conjugated polymers *via* the topochemical polymerization of 1,3-butadiyne moieties, yielding polydiacetylenes (PDA).[15–17] This approach capitalizes on the unique alternating alkene–alkyne backbone of polydiacetylenes, which cannot only impact the thermomechanical properties of the polymers, but also potentially extend π-conjugation across the entire polymer network after crosslinking. The process involves a regioselective 1,4-addition mechanism between adjacent diacetylene units, initiated by UV irradiation and guided by specific structural parameters through supramolecular self-assembly.[18] Moreover, supramolecular self-assembly, or noncovalent crosslinking, can facilitate intermolecular crosslinking in semiconducting polymers without disrupting chain packing and crystallinity—an essential factor for efficient charge transport. Previous work has explored the incorporation of polydiacetylene crosslinks *via* side-chain and backbone engineering – specifically, by integrating diacetylene units into the side chains of the semiconducting polymers or in conjugation breaking units.[15–17] Although Raman spectroscopy confirmed the formation of polydiacetylene crosslinks, the resulting species exhibited often low molecular weight resulting from the intrinsic low solubility of PDAs.

Herein, we report the synthesis and topochemical polymerization of a diketopyrrolopyrrole–carbazole conjugated copolymer featuring 1,3-butadiyne moieties incorporated into the carbazole side chain. Upon UV photoirradiation in the solid state, Raman spectroscopy was used to confirm the formation of PDA crosslinks. Both atomic force microscopy (AFM) and grazing incidence wide-angle X-ray scattering (GIWAXS) verified that the crosslinking process preserved the thin-film morphology of the conjugated polymer. Quantitative nanomechanical mapping further revealed that PDA formation significantly modulates the mechanical properties, as evidenced by changes in Young's moduli. Moreover, solvent resistance experiments – conducted through sequential deposition and crosslinking cycles – demonstrated that new layers could be deposited without compromising the integrity of underlying films, as shown by UV-vis spectroscopy. Collectively, these findings underscore the promise of topochemical polymerization of diacetylenes as a robust strategy for tailoring the mechanical and solvent-resistant properties of conjugated polymers, paving the way for advanced multilayer organic electronic devices.

Results and discussion

To access new PDA-crosslinked semiconducting polymer with high crosslinking density and optimal film formation, a diketopyrrolopyrrole–carbazole copolymer system was chosen due to specific reasons. First, this system allowed for the incorporation of one crosslinkable side-chain per repeating unit while keeping the possibility to have two long branched solubilizing side chains to help with solubility and film formation. Moreover, several DPP–carbazole copolymers were previously reported to possess high charge carrier mobility in organic field-effect transistor and favourable electronic properties in organic photovoltaics, which is important in the context of the development of multilayered organic electronics.[19–22] Importantly, the 1,3-butadiyne side chain used was designed to incorporate an amide moiety. This is not naïve as numerous studies performed on isoindigo-based conjugated polymers, phenylacetylene macrocycles and small-molecule gelators have demonstrated that intermolecular hydrogen bonding is essential for guiding supramolecular self-assembly and enabling the topochemical polymerization of diacetylene units.[15–17,23] In particular, the presence of hydrogen-bonding amide functionalities has been shown to promote the aligned molecular packing required for efficient photopolymerization in isoindigo-based polymers, whereas analogous systems lacking these supramolecular interactions fail to undergo crosslinking under identical conditions.

The synthetic pathway to diyne-containing semiconducting polymer **P1** is depicted in Scheme 1. The complete synthetic procedures and characterizations are also detailed in the ESI.† Briefly, compound **1**, synthesized according to previously reported procedures was added to commercially-available 2,7-dibromocarbazole through alkylation conditions with potassium *tert*-butoxide in THF to afford compound **2** in moderate yields. Compound **2** was subsequently polymerized along with 2,5-bis(2-decyltetradecyl)-3,6-bis(5-(tributylstannyl)thiophen-2-yl)-2,5-dihydropyrrolo[3,4-*c*]pyrrole-1,4-dione under Stille cross-coupling conditions. The reaction mixture was then precipitated in methanol and loaded into a glass thimble. This was then placed within a Soxhlet apparatus in order to subject the polymer to successive extractions with methanol, acetone, hexanes, and chloroform. The resulting fractions were collected and precipitated out in methanol and filtered under vacuum to yield **P1** as dark green solid. The polymer structure was confirmed through ^{1}H NMR, as detailed in ESI.† Notably, as detailed in ESI,† polymer **P2** was also synthesized as a reference

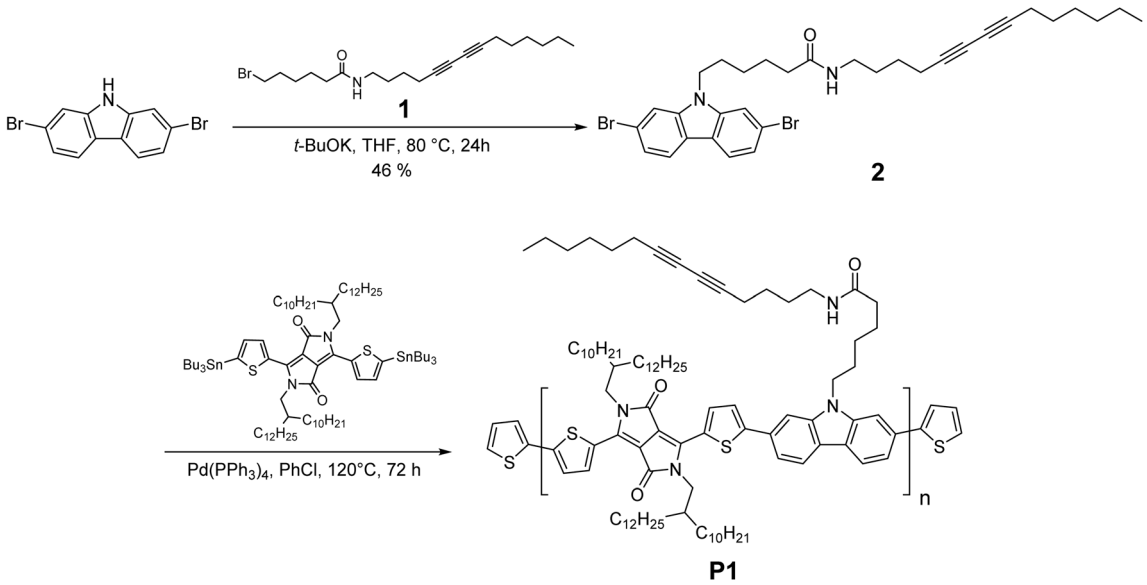

Scheme 1 Synthetic pathway to diacetylene containing polymer **P1**.

polymer to better examine the effects of PDA crosslinks on the mechanical properties and solubility.

The molecular weight analysis of this polymer was done through high-temperature gel-permeation chromatography (HT-GPC). The results of this experiment are summarized in Table 1. The number-average molecular weight M_n and the weight-average molecular weight M_w of **P1** were 5551 g mol^{-1} and 6195 g mol^{-1} respectively. The PDI of this polymer was found to be 1.12. Subsequently, physical characterization of both polymers **P1** and **P2** was performed, and the results are summarized in Table 1. All the experimental details are provided in ESI.† First, the energy levels were determined by cyclic voltammetry (Fig. S9†) and UV-vis spectroscopy (Fig. 1c, S10 and S11†).[24] As expected, both polymers presented similar bandgap and HOMO/LUMO levels, also in agreement with previously reported values.[20,21] Finally, both polymers showed a good thermal stability, as determined by thermogravimetric analysis (Fig. S12†).

As previously reported for other topochemical photopolymerizations that yield PDAs, the supramolecular self-assembly of monomer units plays a crucial role in achieving a high degree of polymerization.[17] In non-crystalline materials, effective self-assembly is often promoted by incorporating hydrogen-bonding moieties adjacent to the 1,3-butadiyne groups.[15–17,23] To investigate the formation and influence of intermolecular hydrogen bonds between adjacent polymer side-chains on the topochemical photopolymerization, Fourier-transform infrared (FTIR) spectroscopy was performed on cast films of polymer **P1**. Intermolecular hydrogen bonding can be identified through the characteristic amide stretching vibrations typically observed in the 3300–3350 cm^{-1} region. Within this spectral region, peaks associated with bonded amide (hydrogen bonding) typically appear between 3300 and 3325 cm^{-1}, while those corresponding to non-bonded amide moieties appear between 3325 and 3350 cm^{-1}.[25–30] As depicted in Fig. 1a and S13,† **P1** exhibited a broad peak centered at approximately 3305 cm^{-1}, confirming both the presence of amide functionalities and indicating that these groups predominantly participate in intermolecular hydrogen bonding interactions in the solid state. In contrast, the reference polymer **P2**, an alkylated derivative, displayed a typical FTIR spectrum characteristic of DPP-based polymers without peaks associated with amide functionalities (Fig. S14†).[26] These findings confirmed the presence of intermolecular hydrogen bonding between polymer chains, potentially contributing to establishing the precise topochemical conditions required for effective polymerization of the diacetylene moieties.

Table 1 Molecular weight, polydispersity, optical properties, and energy levels of **P1** and **P2**

Polymer	M_n[a] (g mol^{-1})	M_w[a] (g mol^{-1})	$Đ_w$[b]	$\lambda_{max\,(film)}$[c] (nm)	E_g^{opt}[d] (eV)	HOMO[e] (eV)	LUMO[f] (eV)
P1	5551	6195	1.12	636	1.40	−5.17	−3.77
P2	6886	7650	1.11	642	1.56	−5.15	−3.59

[a] Number-average molecular weight and weight-average molecular weight estimated by high-temperature gel permeation chromatography in 1,2,4-trichlorobenzene at 180 °C using polystyrene as standard. [b] Weight dispersity defined as M_w/M_n. [c] Absorption maxima determined from drop-casted thin film. [d] Calculated by the following equation: gap = $1240/\lambda_{onset}$ of polymer film. [e] Calculated from cyclic voltammetry (potentials *vs.* Ag/AgCl) using 0.1 M $TBAPF_6$ in CH_3CN as electrolyte. [f] Estimated from calculated E_g^{opt} and HOMO.

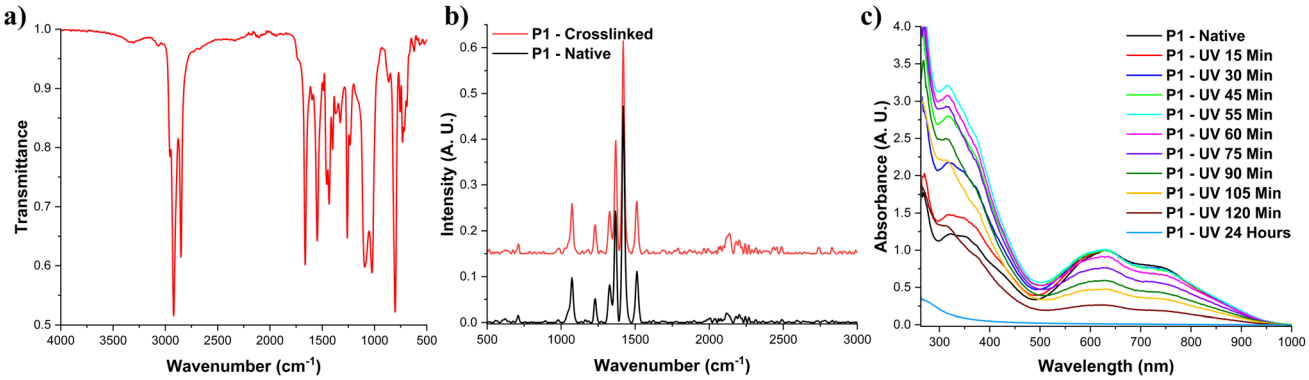

Fig. 1 Characterization of the polymers after photoirradiation. (a) FTIR spectra of **P1**; (b) Raman spectra of **P1**, and (c) solid-state UV-vis spectra of **P1** upon various irradiation time.

Upon photoirradiation of polymer thin films, as detailed in the ESI,† Raman spectroscopy was employed to confirm the formation of polydiacetylene crosslinks between the semiconducting polymer chains. Raman spectroscopy is often the preferred technique for characterizing PDA-containing materials due to its high sensitivity to alkene and alkyne functional groups, a sensitivity not consistently matched by FTIR spectroscopy.[31] Therefore, solid-state Raman spectroscopy was performed on UV-irradiated thin films of polymers **P1** and **P2**, with results presented in Fig. 1b and S15† respectively. For **P1**, two distinct peaks appeared at approximately 1512 and 2136 cm^{-1}, corresponding to alkene and alkyne functionalities, respectively.[32] Given the relatively low intensity of these peaks, Raman analysis was also conducted on monomeric compound **2**, which similarly contains a 1,3-butadiyne side-chain. As shown in Fig. S16,† analogous peaks at 1450 and 2090 cm^{-1} emerged upon photoirradiation, confirming the formation of PDA within the monomer. This result indirectly validates PDA crosslink formation in polymer **P1**. Notably, compound **2** exhibited an additional peak at 2256 cm^{-1} prior to UV irradiation, characteristic of the unreacted 1,3-butadiyne functional group. The simultaneous presence of alkene and alkyne-associated peaks before crosslinking indicates the occurrence of Raman-induced photopolymerization, a phenomenon previously observed for similar materials.[32] Conversely, as shown in Fig. S15,† reference polymer **P2** displayed no detectable diyne peak near 2200 cm^{-1} in its Raman spectrum prior to irradiation, consistent with the absence of diacetylene moieties. These Raman spectroscopy findings conclusively demonstrate the presence of diacetylene groups in both compound **2** and polymer **P1**, as well as their covalent crosslinking into PDA structures upon photoirradiation.

To gain insight into how PDA crosslinks influence the optoelectronic properties of the semiconducting polymers, UV-vis spectroscopy was first conducted at various irradiation intervals (up to 60 minutes), and the resulting spectra are presented in Fig. 1c. Polymer **P1** exhibited a characteristic absorption maximum centered around 650 nm, corresponding to the donor–acceptor charge transfer.[17] Additionally, another absorption peak was observed at approximately 350 nm, associated with the π–π* transition.[17] Upon photoirradiation, a progressive increase in intensity at the 350 nm peak was noted, attributed to the formation of π-conjugated PDA crosslinks.[30] Conversely, the broad absorption band at 650 nm remained essentially unchanged after irradiation periods of up to 55 minutes, confirming the structural stability of the π-conjugated semiconducting backbone under UV exposure. Interestingly, extending irradiation to 60 minutes resulted in a slight decrease in intensity at the 350 nm absorption peak. Beyond this point, a gradual decrease in both absorption bands centered at 350 and 650 nm was observed. After 24 hours of continuous exposure, complete disappearance of the bands was confirmed, which can be attributed to polymer photobleaching caused by prolonged UV irradiation—a phenomenon previously observed in related π-conjugated systems.[16] Similarly, the thermal stability of the polymer was assessed by heating it to 150 °C, above the typical thermal limits of substrates used in printing. UV-vis spectroscopy was used to monitor changes in the polymer's optical properties, and the results are depicted in Fig. S10.† In line with previous thermogravimetric analysis reported for similar systems, the polymer in thin-film form exhibited good thermal stability upon annealing, retaining its optical characteristics for up to 2 hours. After 24 hours of continuous heating, a complete disappearance of the absorption bands centered at 650 nm was observed, which can be attributed to polymer degradation.

Upon confirming the presence of PDA crosslinks in **P1** and the initial characterization of the effect on the optoelectronic properties, additional characterizations were performed to reveal the solid-state nanostructure of the polymer in thin film upon photoirradiation. The polymer morphology is particularly critical for applications in organic electronics, as solid-state assembly often dictates both charge transport and mechanical properties of the polymer.[33] First, to probe for the influence of the topochemical polymerization on the solid-state morphology and the structural organization of the polymers, grazing incidence wide-angle X-ray scattering (GIWAXS) was used. The complete procedure to perform this characterization is detailed in ESI,† and both 1D and 2D patterns are depicted in Fig. 2a, b, S17 and S18.† **P1**, before crosslinking, was shown to be

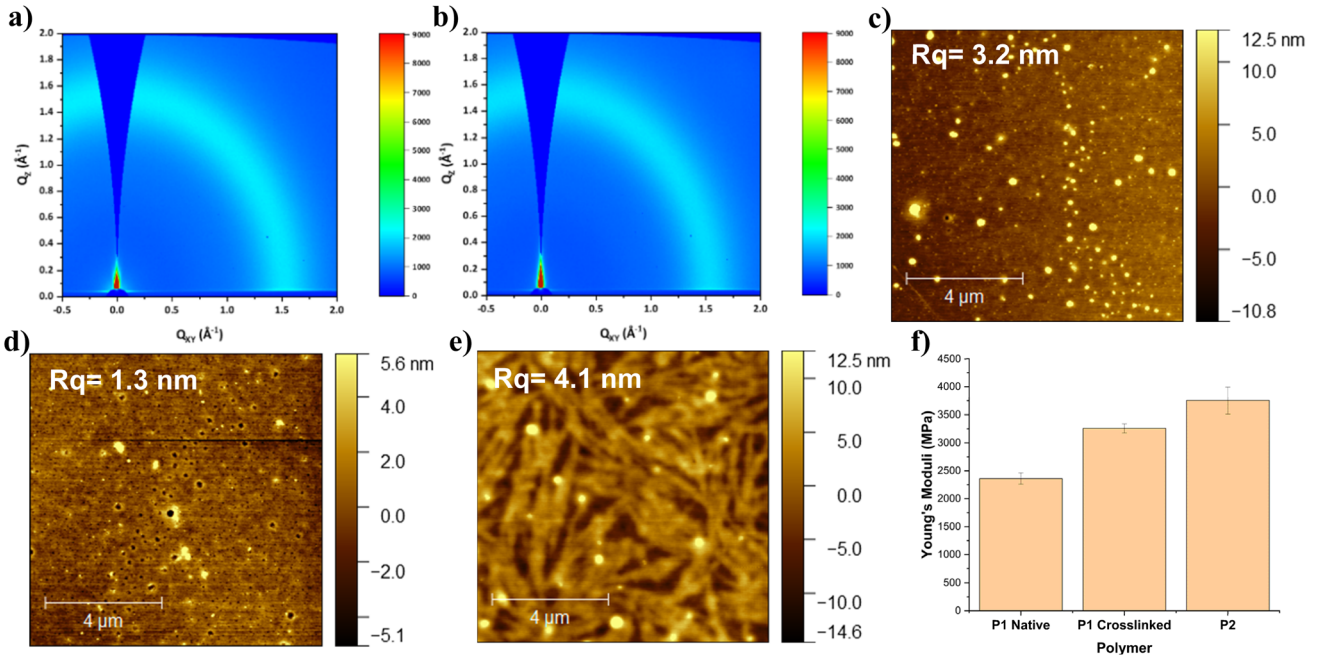

Fig. 2 Impact of photocrosslinking on surface nanostructure and mechanical properties. 2D grazing incidence wide-angle X-ray scattering (GIWAXS) images of thin films of **P1** (a) before and (b) after UV irradiation, and atomic force microscopy (AFM) height images with root-mean-square (R_q) surface roughness for (c) **P1** before UV irradiation, (d) **P1** after 1 hour of UV irradiation, and (e) **P2**; (f) bar graph showing trend in Young's modulus of **P1**, before and after crosslinking, and **P2**.

amorphous both in the out-of-plane and in-plane directions, with the absence of notable reflections that can be attributed to lamellar spacing or π–π stacking, typically observed for other semicrystalline conjugated polymers.[15–17] Upon photo-irradiation, the polymer nanostructure remained amorphous, indicating that the photocrosslinking does not seem to promote the formation of crystalline domain or different morphology in the solid-state. This was expected as the formation of PDA occurs through a topochemical photopolymerization that results in no structure changes.[16,17] In contrast to **P1**, GIWAXS revealed that reference polymer **P2** is semicrystalline, as indicated by the presence of several features associated to the 100, 200, and 300 reflections in the out of plane direction. Primarily assembled in an edge-on orientation, **P2** showed a lamellar *d*-spacing of 26.49 Å. This clear difference in crystallinity can be attributed to the presence of the amide functional groups in **P1**. While these functional groups can enable the formation of intermolecular hydrogen bonding, they also disrupt the side-chain interdigitation, leading to a net decrease in crystallinity. This phenomenon has been observed by us and others in similar systems.[34,35] The presence of the 1,3-butadiyne cannot also be ruled out to be detrimental to the formation of highly crystalline domains in the solid-state.

In addition to GIWAXS characterization, atomic force microscopy (AFM) was employed to further investigate the solid-state morphology of the semiconducting polymer both before and after crosslinking. As shown in Fig. 2c, d and S19,† AFM images of **P1** (thin film obtained *via* spin-coating) revealed a relatively smooth surface, lacking distinct or well-defined domains, with a calculated root mean square (RMS) roughness of 3.2 nm. After crosslinking, the polymer surface remained smooth and homogeneous, showing no evidence of aggregates or defined nanoscale structures. The RMS roughness slightly decreased to 1.3 nm, indicating minimal morphological disruption resulting from the crosslinking. To elucidate the influence of molecular design and crosslinking on surface morphology, AFM measurements were also performed on the reference polymer, **P2** (Fig. 2e). In contrast to **P1**, the AFM height image of **P2** revealed well-defined fibrillar structures along with sparse, small aggregates. This resulted in a moderately higher RMS roughness value of 4.1 nm. These morphological observations are consistent with the GIWAXS findings, which indicated that **P2** exhibits a semicrystalline nature, whereas **P1** displays predominantly amorphous characteristics. Overall, AFM results highlight the significant role side-chain design plays in defining polymer morphology. Additionally, the data confirms that the nanoscale morphology of **P1** is largely preserved following covalent crosslinking *via* diacetylene units, resulting in polydiacetylene crosslinks.

In addition to probing nanoscale morphology, AFM was utilized to investigate the mechanical properties of polymer films before and after crosslinking. Quantitative nano-mechanical mapping (QNM) employing the Derjaguin–Muller–Toporov (DMT) contact mechanics model was conducted to determine the compression Young's modulus, providing valuable insights into nanoscale mechanical and surface properties.[36] The detailed sample preparation and experimental procedures are described in the ESI,† with results depicted in Fig. S20 and Table S1,† and summarized in Fig. 2f. Before crosslinking, polymer **P1** exhibited a Young's modulus of

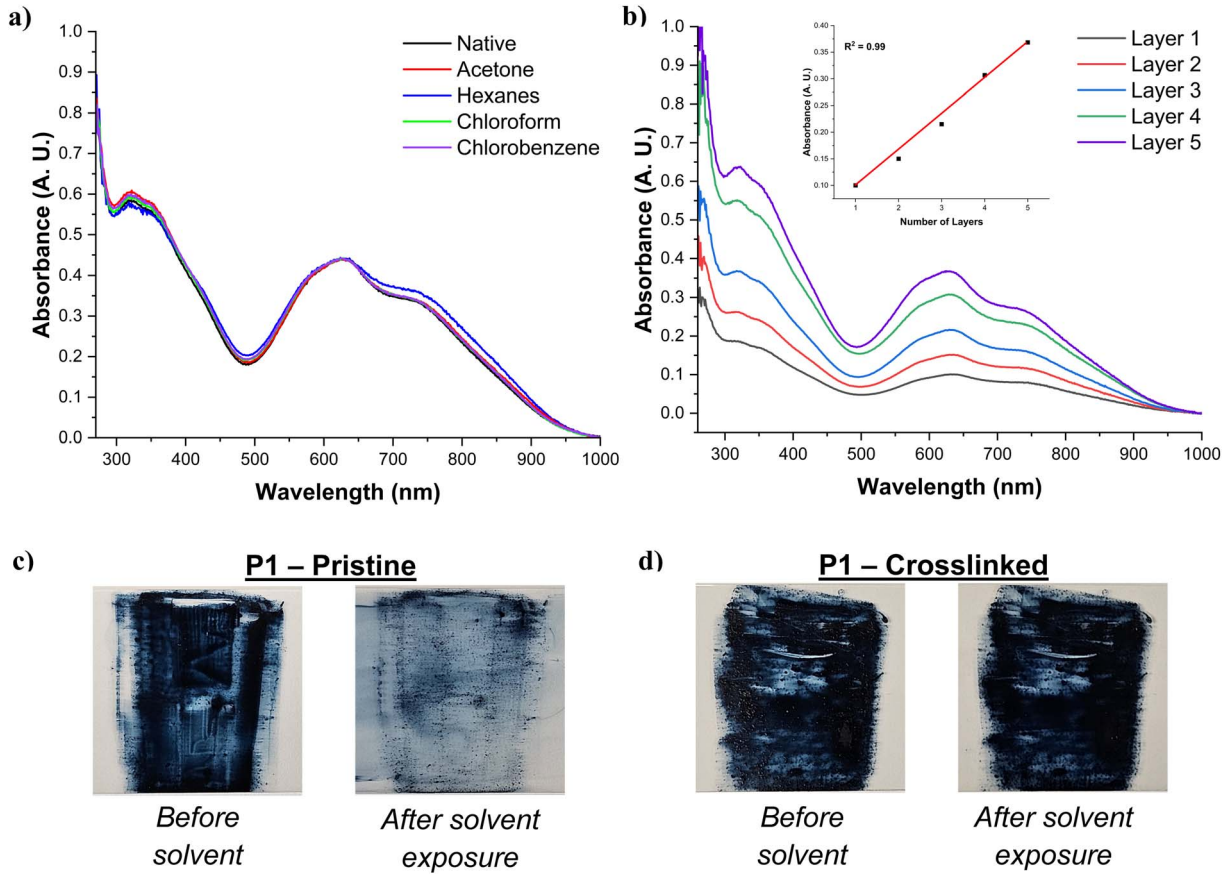

Fig. 3 Investigating solvent resistance of the PDA-crosslinked semiconducting polymers. (a) UV-vis spectra of **P1** after immersion in several common organic solvents, and (b) UV-vis spectra of layer-by-layer deposition of **P1** (inset figure represents the relationship between the number of layers and the absorbance at lambda max); demonstration of the solvent resistant properties of (c) a cast film of **P1** (pristine) before and after immersion in chlorobenzene for 1 minute and (d) a cast film of **P1** (crosslinked) before and after immersion in chlorobenzene for 1 minute.

2360 MPa, aligning closely with values previously reported for similar semiconducting polymers.[17] After crosslinking, the modulus increased to 3260 MPa, indicative of enhanced rigidity probably due to intermolecular crosslinks formed within the polymer network. For comparison, the control polymer **P2** displayed a higher modulus of 3753 MPa, attributed primarily to its increased crystallinity, as previously evidenced by X-ray scattering and AFM analyses. These observations emphasize the crucial roles of molecular design and crystallinity on governing the mechanical properties of polymer thin films. More importantly, these results also confirm the potential of this new crosslinking methodology in achieving more robust thin film and related electronics.

As demonstrated previously, the formation of PDA crosslinks through topochemical photopolymerization of the 1,3-butadiyne units present in the side chains of polymer **P1** has negligible effects on its optoelectronic and solid-state characteristics. This unique feature makes PDA crosslinking particularly attractive for engineering solvent resistance postprocessing, potentially facilitating the fabrication of multilayered organic electronic devices using solution-based methods. Typically, solution-processed semiconducting thin films exhibit substantial solubility in common organic solvents, especially halogenated or aromatic ones, posing substantial challenges when sequentially depositing layers due to dissolution or interlayer mixing.[11,37] The solvent resistance induced by PDA crosslinking, evidenced by a marked decrease in solubility following UV irradiation, can effectively resolve these issues by preserving the integrity of each layer during multilayer deposition. Moreover, unlike alternative solvent resistance methods – which usually involve chemical or thermal deprotection of solubilizing groups that can be detrimental to the polymer electronic, mechanical or solid-state properties – UV-induced crosslinking offers distinct advantages for large-scale manufacturing, including the potential for high-throughput and cost-effective production. To validate the solvent-resistant properties of crosslinked **P1** films, we initially examined their stability in several common organic solvents using UV-vis spectroscopy. As depicted in Fig. 3a, S21 and S22,† the photocrosslinked **P1** films exhibited no noticeable changes in their optoelectronic properties, indicating excellent stability. In contrast, polymer **P2** quickly dissolved in most tested solvents, clearly evidenced either by a significant loss of absorbance and/or film delamination (Fig. S23†). Further exploring the practical utility of this method, we utilized a sequential layer-by-layer spin-coating approach (described in ESI†) to confirm the

successful deposition of discrete, non-intermixing polymer layers, monitoring the process with UV-vis spectroscopy (Fig. 3b). Films were consistently prepared through repetitive casting and photocrosslinking cycles, recording UV-vis absorbance after each step. Due to uniform polymer concentration and consistent deposition conditions, increases in absorbance accurately reflect each newly added layer's uniform thickness. Our observations showed a highly linear relationship between the absorbance and the number of deposited layers ($R^2 = 0.99$), confirming the formation of distinct layers free from solvent-induced intermixing. This robust methodology not only underscores the exceptional solvent resistance imparted by PDA crosslinking in polymer **P1** but also demonstrates its considerable potential for creating multilayer semiconductor devices with precise control over layer thickness and composition.

Conclusion

In summary, a new DPP–carbazole copolymer containing diacetylene units within its side chains was designed and synthesized. The semiconducting polymer was topochemically polymerized *via* UV irradiation to create polydiacetylene crosslinks between adjacent polymer chains, as confirmed by Raman spectroscopy. AFM and GIWAXS analyses demonstrated that the structural morphology of the polymer backbone remained intact following polymerization, underscoring the topochemical nature of the reaction. By directly comparing this polymer to an analogous DPP-based polymer lacking diacetylene groups, we observed that the diyne-containing polymer exhibited a notably more amorphous character compared to the more crystalline nature of the control polymer. Quantitative nanomechanical mapping revealed a significant increase in the Young's modulus, going from 2360 MPa before crosslinking to 3260 MPa after crosslinking, indicating enhanced stiffness and rigidity resulting directly from the polydiacetylene crosslink formation. These observations collectively affirm that integrating diacetylene moieties into the polymer side chains effectively modulates mechanical properties, rendering the polymer more amorphous and mechanically tunable. Finally, the incorporation of PDA crosslinks through topochemical photopolymerization of 1,3-butadiyne side chains was shown to trigger solvent resistance while minimally impacting the optoelectronic properties of the polymer, which was investigated through UV-vis spectroscopy. This approach enables precise, controlled multilayer deposition without intermixing, demonstrating great promise for the fabrication of advanced multilayer organic electronic devices. Overall, this study clearly demonstrates the utility of topochemical diacetylene polymerization as a versatile approach for tailoring mechanical properties in conjugated polymer systems while enabling new properties such as solvent resistance, opening new avenues for the large-scale fabrication of multilayered multifunctional organic electronics. Moreover, this approach holds broad potential for extension to other classes of materials, particularly in applications where post-deposition crosslinking and enhanced film durability are critical.

Data availability

The data supporting this article have been included as part of the ESI.†

Author contributions

All authors contributed to the manuscript. All authors have given approval to the final version of the manuscript.

Conflicts of interest

The authors declare no competing financial interest.

Acknowledgements

This work was supported by the Natural Sciences and Engineering Research Council of Canada (NSERC) through a Discovery Grant (RGPIN-2022-04428) and an Alliance International Catalyst grant (590450-2023). S. R.-G. acknowledges financial support from the Canada Foundation for Innovation (CFI), the Ontario Research Fund, and the University of Windsor. A. N. thanks NSERC for financial support through a Postgraduate Scholarship – Doctoral. The author would like to thank Mark Potter (UWindsor) for help with thermogravimetric analysis and Matthew Revington (UWindsor) for help with NMR spectroscopy. The author would also like to thank Dr M. Nazir Tahir and Dr Tiago Gomes (both at UWindsor) for help in synthesis and materials characterizations. The author also thanks Dr Garima Garg and Gage T. Mason (both at UWindsor) for help with polymer characterization through gel-permeation chromatography.

References

1 J. A. Rogers and Z. Bao, *J. Polym. Sci., Part A: Polym. Chem.*, 2002, **40**, 3327–3334.
2 X. Guo, M. Baumgarten and K. Müllen, *Prog. Polym. Sci.*, 2013, **38**, 1832–1908.
3 Z. Nie and E. Kumacheva, *Nat. Mater.*, 2008, **7**, 277–290.
4 F.-J. Kahle, C. Saller, A. Köhler and P. Strohriegl, *Adv. Energy Mater.*, 2017, **7**, 1700306.
5 X. Wang, J. Deng, X. Duan, D. Liu, J. Guo and P. Liu, *J. Mater. Chem. A*, 2014, **2**, 12323–12329.
6 J. Freudenberg, D. Jänsch, F. Hinkel and U. H. F. Bunz, *Chem. Rev.*, 2018, **118**, 5598–5689.
7 M. J. Kim, M. Lee, H. Min, S. Kim, J. Yang, H. Kweon, W. Lee, D. H. Kim, J.-H. Choi, D. Y. Ryu, M. S. Kang, B. Kim and J. H. Cho, *Nat. Commun.*, 2020, **11**, 1520.
8 A. X. Chen, J. D. Hilgar, A. A. Samoylov, S. S. Pazhankave, J. A. Bunch, K. Choudhary, G. L. Esparza, A. Lim, X. Luo, H. Chen, R. Runser, I. McCulloch, J. Mei, C. Hoover, A. D. Printz, N. A. Romero and D. J. Lipomi, *Adv. Mater. Interfaces*, 2023, **10**, 2202053.
9 C. Gao, D. Shi, C. Li, X. Yu, X. Zhang, Z. Liu, G. Zhang and D. Zhang, *Adv. Sci.*, 2022, **9**, 2106087.

10 N. Reddy, R. Reddy and Q. Jiang, *Trends Biotechnol.*, 2015, **33**, 362–369.
11 M. Mooney, Y. Wang, E. Iakovidis, X. Gu and S. Rondeau-Gagné, *ACS Appl. Electron. Mater.*, 2022, **4**, 1381–1390.
12 B. Schmatz, Z. Yuan, A. W. Lang, J. L. Hernandez, E. Reichmanis and J. R. Reynolds, *ACS Cent. Sci.*, 2017, **3**, 961–967.
13 B. V Khau, L. R. Savagian, M. De Keersmaecker, M. A. Gonzalez and E. Reichmanis, *ACS Mater. Lett.*, 2019, **1**, 599–605.
14 C. R. Harding, J. Cann, A. Laventure, M. Sadeghianlemraski, M. Abd-Ellah, K. R. Rao, B. S. Gelfand, H. Aziz, L. Kaake, C. Risko and G. C. Welch, *Mater. Horiz.*, 2020, **7**, 2959–2969.
15 A. Nyayachavadi, G. T. Mason, M. Nazir Tahir, M. U. Ocheje and S. Rondeau-Gagné, *Langmuir*, 2018, **34**, 12126–12136.
16 A. Nyayachavadi, A. Langlois, M. N. Tahir, B. Billet and S. Rondeau-Gagné, *ACS Appl. Polym. Mater.*, 2019, **1**, 1918–1924.
17 A. Nyayachavadi, A. K. Sur, P. Kulatunga, Y. Wang, T. C. Gomes, M. Mooney, G. T. Mason, A. Hu, X. Gu and S. Rondeau-Gagné, *Chem. Mater.*, 2023, **35**, 9682–9691.
18 G. Wegner, *Macromol. Chem. Phys.*, 1972, **154**, 35–48.
19 L. Yang, Y. Yu, J. Zhang, F. Chen, X. Meng, Y. Qiu, Y. Dan and L. Jiang, *Appl. Surf. Sci.*, 2018, **434**, 796–805.
20 S. Chen, B. Sun, W. Hong, Z. Yan, H. Aziz, Y. Meng, J. Hollinger, D. S. Seferos and Y. Li, *J. Mater. Chem. C*, 2014, **2**, 1683–1690.
21 H. Opoku, B. Lim, E. Shin, H. Kong, J. M. Park, C. Bathula and Y. Noh, *Macromol. Chem. Phys.*, 2019, **220**, 1900287.
22 Y. Zhu, A. R. Rabindranath, T. Beyerlein and B. Tieke, *Macromolecules*, 2007, **40**, 6981–6989.
23 J. W. Lauher, F. W. Fowler and N. S. Goroff, *Acc. Chem. Res.*, 2008, **41**, 1215–1229.
24 P. Acevedo-Peña, A. Baray-Calderón, H. Hu, I. González and V. M. Ugalde-Saldivar, *J. Solid State Electrochem.*, 2017, **21**, 2407–2414.
25 W. J. Mullin, S. A. Sharber and S. W. Thomas III, *J. Polym. Sci.*, 2021, **59**, 1643–1663.
26 M. U. Ocheje, B. P. Charron, Y.-H. Cheng, C.-H. Chuang, A. Soldera, Y.-C. Chiu and S. Rondeau-Gagné, *Macromolecules*, 2018, **51**, 1336–1344.
27 S. I. Stupp and L. C. Palmer, *Chem. Mater.*, 2014, **26**, 507–518.
28 Y. Ma, H. Niu, X. Zhang and Y. Cai, *Analyst*, 2011, **136**, 4192–4196.
29 H. Luo, C. Gu, W. Zheng, F. Dai, X. Wang and Z. Zheng, *RSC Adv.*, 2015, **5**, 13470–13477.
30 R. Thota and V. Ganesh, *RSC Adv.*, 2016, **6**, 49578–49587.
31 J. Huo, Z. Hu, G. He, X. Hong, Z. Yang, S. Luo, X. Ye, Y. Li, Y. Zhang, M. Zhang, H. Chen, T. Fan, Y. Zhang, B. Xiong, Z. Wang, Z. Zhu and D. Chen, *Appl. Surf. Sci.*, 2017, **423**, 951–956.
32 R. H. Baughman, J. D. Witt and K. C. Yee, *J. Chem. Phys.*, 1974, **60**, 4755–4759.
33 I. Osaka and K. Takimiya, *Polymer*, 2015, **59**, A1–A15.
34 B. P. Charron, M. U. Ocheje, M. Selivanova, A. D. Hendsbee, Y. Li and S. Rondeau-Gagné, *J. Mater. Chem. C*, 2018, **6**, 12070–12078.
35 M. U. Ocheje, M. Selivanova, S. Zhang, T. H. Van Nguyen, B. P. Charron, C.-H. Chuang, Y.-H. Cheng, B. Billet, S. Noori and Y.-C. Chiu, *Polym. Chem.*, 2018, **9**, 5531–5542.
36 P. Kulatunga, M. Comí, T. C. Gomes, M. Seifi, R. Majidzadeh, M. Al-Hashimi and S. Rondeau-Gagné, *J. Mater. Chem. C*, 2023, **11**, 14661–14670.
37 C. Newby, J.-K. Lee and C. K. Ober, *Macromol. Res.*, 2013, **21**, 248–256.